

CAMul: Calibrated and Accurate Multi-view Time-Series Forecasting

Harshavardhan Kamarthi, Lingkai Kong, Alexander Rodríguez, Chao Zhang, B. Aditya Prakash
College of Computing

Georgia Institute of Technology

{harsha.pk, lkkong, arodriguez, chaozhang, badityap}@gatech.edu

Abstract

Probabilistic time-series forecasting enables reliable decision making across many domains. Most forecasting problems have diverse sources of data containing multiple modalities and structures. Leveraging information as well as uncertainty from these data sources for well-calibrated and accurate forecasts is an important challenging problem. Most previous work on multi-modal learning and forecasting simply aggregate intermediate representations from each data view by simple methods of summation or concatenation and do not explicitly model uncertainty for each data-view. We propose a general probabilistic multi-view forecasting framework CAMUL, that can learn representations and uncertainty from diverse data sources. It integrates the knowledge and uncertainty from each data view in a dynamic context-specific manner assigning more importance to useful views to model a well-calibrated forecast distribution. We use CAMUL for multiple domains with varied sources and modalities and show that CAMUL outperforms other state-of-art probabilistic forecasting models by over 25% in accuracy and calibration.

1 Introduction

Time-series forecasting is a classic machine learning problem with applications covering wide-ranging domains including retail, meteorology, economics, epidemiology and energy. For many of these applications, we have a wide variety of datasets representing different *views* or perspectives of the phenomena to forecast. These views may differ in their structure and modality, and also in the quality and reliability associated due to collection and processing differences. Due to the high-stakes decisions that these forecasts may inform (e.g., hospital resource allocation for COVID-19), designing ML models that can leverage these multiple data sources to provide not only accurate but also well-calibrated forecast distributions is an important task.

State-of-the-art time series forecasting methods employ sequential neural models that can naturally integrate multiple time-varying exogenous features (Salinas et al. 2020; Li et al. 2021; Rangapuram et al. 2018). However, they are not suitable to ingest multiple modalities of data such as networks, sequences and fixed sized features together.

Effective integration of information from multiple views is challenging because information from individual views may be noisy, conflicting, redundant or sometimes unreliable. Recent works that seek to integrate multi-source and multi-modal data for accurate sequence forecasting by using architectures like Graph Neural networks and Convolutional networks (such as for disease (Ramchandani, Fan, and Mostafavi 2020) and sales forecasting (Ekambaram et al. 2020)) do not comprehensively address this challenge. They propose to combine embeddings from multiple data sources either through direct concatenation (Hu et al. 2020) or simple summation (Ramchandani, Fan, and Mostafavi 2020). Other recent methods (Chen et al. 2021a) learn a data-view-specific importance parameter and use it to combine embeddings in a weighted manner. However, these weights are learned over all data-points and are not context-sensitive: they do not account for temporal variation in the importance of each view as well as variance across time series.

Moreover, these multi-modal time-series forecasting methods do not focus on learning a *well-calibrated* forecast distribution. This is especially challenging in a multi-view setting since the ambiguity and reliability of views has to be integrated to better inform forecast uncertainty. Redundancy and high confidence in beliefs across multiple data views could inform a more confident forecast whereas conflicting information and lower confidence from some data sources may suggest higher uncertainty. Past works on multi-view probabilistic forecasting (Yan et al. 2021) do not integrate stochastic information about beliefs from individual data views and instead use a deterministic embedding from fusion of view-specific embeddings to learn distribution parameters. As a result, these methods do not model the view-specific uncertainty which may result in mis-calibrated forecasts.

Hence in this paper, our work tackles the challenge of modelling as well as integrating information and uncertainty from each data view to provide accurate and well-calibrated time-series forecasts (Figure 1). We introduce a general multi-view probabilistic time-series forecasting framework, CAMUL (Calibrated and Accurate Multi-view Forecasting, pronounced ‘camel’), that jointly models uncertainty from multiple views independently using a latent embedding distribution. It then combines them in a context-sensitive mechanism accounting for unreliable data views specific to given sequence to provide a well-calibrated and accurate forecasts.

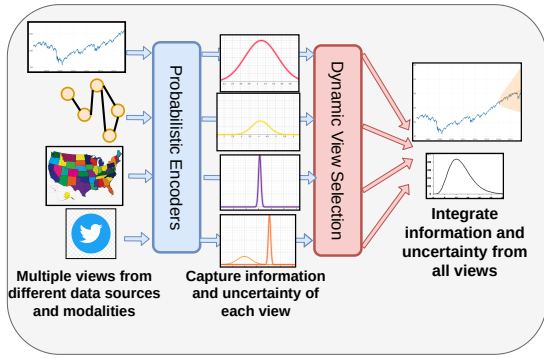


Figure 1: CAMUL models and integrates view-specific information and uncertainty.

To learn a view-specific distribution capturing relevant information for each data source, we use a non-parametric modelling framework. We directly use latent embeddings of datapoints in the training set of each view in the functional space to allow flexible representation of the predictive distribution that rely on similar patterns seen before. Our main contributions are:

- a) **Probabilistic Neural Framework jointly modeling multi-view uncertainty:** We propose a general framework CAMUL for probabilistic time series forecasting on multi-modal and multi-source data. We make no assumptions on the structure of data. Our non-parametric generative model leverages probabilistic relations learned between latent representations of data points for each data view independently accounting for uncertainty from each view.
- b) **Integrating multi-view uncertainty towards calibrated forecasts:** CAMUL leverages the latent information and uncertainty from each view and carefully integrates the beliefs from multiple views together, dynamically weighting each view’s importance based on input data, to learn well-calibrated predictive distribution.
- b) **Evaluation of CAMUL on multiple domains:** We use the CAMUL framework to design models for multi-view time-series forecasting tasks from different domains using diverse data sources and modalities (static features, sequences, networks). We compare CAMUL against state-of-art domain-specific as well as general forecasting baselines and show that CAMUL models clearly outperform all baselines by over 25% in accuracy and calibration. We also show both empirically and using case studies, that our method of modeling and integrating uncertainty from individual data sources indeed causes these significant improvements.

2 Related Work

Probabilistic Time-series Forecasting Classical time-series forecasting like exponential smoothing, ARIMA-based models (Hyndman and Athanasopoulos 2018) focus on univariate time-series with a small number of exogenous features and learn model parameters independently for each sequence. Recent probabilistic forecasting models leverage the representation power of neural sequential modules like DeepAR (Salinas et al. 2020) which directly models the mean and variance parameters of the forecast distribution, Bayesian Neural

Networks (Zhu and Laptev 2017) which require assigning useful priors to parameters and require high computational resources for learning. Other recent works are inspired by classic state-space models like Deep State Space models (Li et al. 2021; Rangapuram et al. 2018). EpiFNP (Kamarthi et al. 2021) a state-of-art calibrated disease forecasting model, is closest to our work and leverages Functional Neural Process (FNP) (Louizos et al. 2019), which uses stochastic correlations between input data and datapoints to model a flexible non-parametric distribution for univariate sequences. Our work leverages FNP for uncertainty modeling of each of the individual views before we jointly model the forecast distribution combining distributions from different views.

Multi-view time-series forecasting Recent advances in deep learning architectures have allowed us to extract and combine representations from multi-modal data sources in an end-to-end fashion. Most methods employ simple summation or concatenation methods (Yan et al. 2021; Li, Yang, and Zhang 2018) to combine representations from multiple sources (Ramchandani, Fan, and Mostafavi 2020; Ekambaram et al. 2020), or use a learned data-source specific weight (Chen et al. 2021a) which does not account for dynamic variation in the importance of each view. In contrast, we model data-view specific uncertainty by learning a latent distribution for each view which allows the model to reason about source specific uncertainty as it integrates uncertainty-aware stochastic representations of all views towards the forecast distribution.

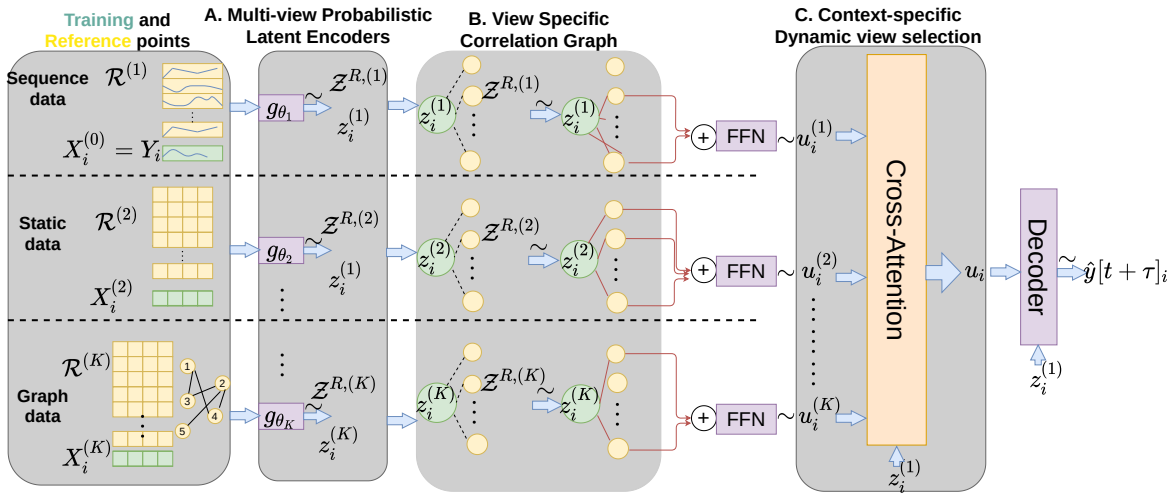
3 Problem Formulation

We describe the *Multi-view probabilistic forecasting* problem, a generalization of the probabilistic forecasting problem to multi-modal and multi-source data. We denote the time-series dataset as $\mathcal{Y} = \{Y_i\}_{i=1}^N$ where individual time-series is a univariate sequence, $Y_i = \{y[t]_i : y[t]_i \in \mathbf{R}, 1 \leq t \leq T\}$. At each time-step t , we also have exogenous data sources that can be used to forecast future values in \mathcal{Y} . We divide these features from multiple sources and modalities into *views*. Assume we have K views for a specific problem representing K sources/modalities of data. The dataset for a view j is denoted by $\mathcal{X}^{(j)} = \{X_i^{(j)}\}_{i=0}^N$. We do not assume any specific data type for each view. However, all datapoints of a view are assumed to have the same type. We can also have *static views* whose values do not change across time: $\forall t, x[t]_i^{(j)} = x[1]_i^{(j)}$. In some cases, we also denote as $X[1 : t]_i^{(j)}$ all the data till week t : $X[1 : t]_i^{(j)} = \{x[t']_i^{(j)} : 0 \leq t' \leq t\}$.

Given the time-series values $\{Y[1 : t]_i\}_{i=0}^N$ and exogenous features from all views $\{X[1 : t]_i^{(j)}\}_{i=1 \dots N, j=1 \dots K}$ till current time t , our goal is to model a well-calibrated forecast probability distribution

$$P(\{y[t + \tau]_i\}_{i=1}^N | \{Y[1 : t]_i\}_{i=1}^N, \{\{X[1 : t]_i^{(j)}\}_{i=1 \dots N, j=1 \dots K}\})$$

for forecasting time-series values $\{y[t + \tau]_i\}_{i=1}^N$, τ steps in future. We also assume that the view 1 is the sequence dataset, i.e, $Y_i = X_i^{(1)}$, $\forall i$ and refer to it as the *default view*.



A: Multi-view Probabilistic Latent Encoder learns probabilistic embeddings for datapoints of each view
 B: View Specific Correlation Graph encodes stochastic relation between input data and reference points that capture global informations of the view
 C: Context-specific Dynamic View Selection module integrates view aware embeddings using context-sensitive importance weights from cross-attention. Decoder uses aggregated embedding to learn output distribution.

Figure 2: Pipeline of our method CAMUL describing all the components of the generative process.

4 Methodology

We first give an overview of CAMUL and then describe each of its modules in more detail.

Model Overview: CAMUL tackles the challenges related to jointly modeling useful information and uncertainty from multiple data-sources. It jointly models the predictive uncertainty by integrating information and uncertainty for each view. It dynamically considers the importance of each view based on input sequence to leverage the more important views and learn the output distribution. We use the functional neural process (FNP) (Louizos et al. 2019) framework to learn a non-parametric latent embedding distribution for each view which enables a flexible method to model complex distribution by leveraging latent similarity with past training data-points from each data view. In contrast to related approaches that use FNP for univariate sequences (Kamarthi et al. 2021), CAMUL solves a more general and harder problem of leveraging stochastic uncertainty from multi-source, multi-modal data and tackles the challenge of jointly modeling and integrating stochastic representations from each view.

At a high level, CAMUL accomplishes our goals by performing the following steps in an end-to-end manner: A) learn latent representations for each view using *Multi-view Latent Probabilistic Encoders* to capture information and uncertainty from each data source, B) leverage stochastic similarity between data-points in latent space to learn relations between time-series for each view via *View Specific Correlation Graph* and leverage these relations to derive a view-aware embedding distribution, C) combine latent embedding distributions from multiple views using learned importance of each view based on input sequence via *Context-sensitive Dynamic View Selection Module* to derive the output distribution. Figure 2 shows the full pipeline.

For each view j , the set of data-points on which we learn the stochastic similarity w.r.t input point is a subset of the training set $\mathcal{X}^{(j)}$ of the view j that comprehensively represents the entire training data. This set is called the *reference*

set, denoted by $\mathcal{R}^{(j)}$. For example, for a view that represents sequence data from the past, we consider each of the complete time-series sequences $X[1 : t]_i^{(j)}$ from past training data as a single data-point in the reference set. Similarly consider views that represent static time-specific data such as months. Each training point for a given month contains the same static features. Therefore, the reference set contains a datapoint for each unique month. Note that, during inference, we retain these reference sets and use them to derive the output distribution.

4.1 Multi-view Probabilistic Latent Encoders

To capture useful information and uncertainty from each view, we learn a latent embedding distribution for datapoints of a specific view. We leverage appropriate neural encoders for each view based on the modality to learn latent distribution parameters. The probabilistic encoder g_{θ_j} for each view j derives the parameters of latent embedding distribution for each of the reference points $\mathcal{R}^{(j)} = \{R_k^{(j)}\}_{k=1}^{N_j}$ and input training point $X_i^{(j)}$ parameterized by a Gaussian Distribution:

$$\begin{aligned} \mu_k^{(j)}, \sigma_k^{(j)} &= g_{\theta_j}(R_k^{(j)}) \\ z_k^{(j)} &\sim \mathcal{N}(\mu_k^{(j)}, \sigma_k^{(j)}). \end{aligned} \quad (1)$$

g_{θ_j} , a neural network module parameterized by θ_j , is chosen based on the modality of view j . For example, we use GRU for views with sequence data, Graph Convolutional Network (Kipf and Welling 2016) to encode relational data and Feed-Forward networks for static fixed-sized features. The Appendix contains detailed discussions of encoder architectures for different views used in this paper. The set of all latent encodings of reference set $\mathcal{R}^{(j)}$ and training set $\mathcal{X}^{(j)}$ is denoted as $\mathcal{Z}^{R,(j)}$ and $\mathcal{Z}^{X,(j)}$ respectively.

4.2 View Specific Correlation Graph

The latent embedding for input data $z_i^{(j)} \in \mathcal{Z}^{X,(j)}$ captures the probabilistic information of input data in view j whereas

latent variables of $\mathcal{Z}^{R,(j)}$ capture stochastic information from entirety of the data view j . To capture the information from entire the data view j conditioned on datapoint i , we use the non-parametric FNP framework that allows modeling a flexible data-view aware latent distribution for given input data by leveraging related reference points of the view.

We first learn probabilistic relations between input datapoint and reference points in latent space using a similarity metric to create a *View Specific Correlation Graph* (VSCG) and then use the reference points connected to input's embedding in VSCG to learn the *view-aware latent embedding*.

We choose the radial basis function (RBF) as the similarity metric to relate reference set $\mathcal{R}^{(j)}$ to training set $\mathcal{X}^{(j)}$:

$$k(z_i^{(j)}, z_k^{(j)}) = \exp(-\rho \|z_k^{(j)} - z_i^{(j)}\|^2). \quad (2)$$

for all $z_k^{(j)} \in \mathcal{Z}^{R,(j)}$ and $z_i^{(j)} \in \mathcal{Z}^{X,(j)}$.

Next, we sample the VSCG $G^{(j)}$ as a bipartite graph between $\mathcal{R}^{(j)}$ and $\mathcal{X}^{(j)}$, modeling each edge as a Bernoulli distribution parameterized by RBF similarity

$$p((i, k) \in G^{(j)}) = \text{Bern}(k(z_i^{(j)}, z_k^{(j)})). \quad (3)$$

Note that during training, we approximate sampling from the discrete Bernoulli using a Gumbel-softmax distribution (Jang, Gu, and Poole 2017). Finally, we aggregate the sampled neighbouring reference points $N(i)$ for each training point i to construct the *view-aware latent variable* $u_i^{(j)}$ (refer Figure 2) as:

$$\begin{aligned} \mu(u_i^{(j)}), \hat{\sigma}(u_i^{(j)}) &= \sum_{k \in N(i)} (l_j^\mu(z_k^{(j)}), l_j^\sigma(z_k^{(j)})) \\ u_i^{(j)} &\sim \mathcal{N}(\mu(u_i^{(j)}), \exp(\hat{\sigma}(u_i^{(j)}))), \end{aligned} \quad (4)$$

where l_j^μ and l_j^σ are linear layers. Thus the view-aware embedding's latent distribution is derived from sampled reference points to capture view-specific information. The stochastic process of VSCG also models view-specific uncertainty.

4.3 Context-Specific Dynamic Views Selection

Not all views are equally useful to learn a well-calibrated forecast distribution. The importance of each view for predictive distribution also varies for each time-series and across time. For instance, for disease prediction, views representing features related to time (like months) may be useful for predicting seasonal changes but its importance may decrease during highly volatile and uncertain weeks near the peak where short-term sequence history and real-time exogenous features are more important. The importance of a view may also change dynamically when the features are corrupted for a small period of time during collection or measurement.

Thus, we need a dynamic mechanism to weigh the importance of each view based on the input sequence. We propose the *View Selection module* to learn importance weights for each view conditioned on input sequence and then aggregate embeddings from multiple views in proportion to learned weights. Given the *view-aware latent variables* of all K views for each datapoint i as $\{u_i^{(j)}\}_{j=1}^K$, we combine these multiple views' knowledge towards the construction

of final functional for predictive distribution. We leverage the cross-attention mechanism from (Vaswani et al. 2017) to learn the importance of each view but also condition the weights on input sequence's representation from default view 1 that encodes the time-series sequence $z_i^{(1)}$ as:

$$\{\alpha_i^{(j)}\}_{j=1}^K = \text{Softmax}_j(\{h_1(z_i^{(1)})^T h_2(u_i^{(j)})\}_{j=1}^K), \quad (5)$$

where h_1 and h_2 are linear layers to transform both embeddings to same dimensions. $\{\alpha_i^{(j)}\}_{j=1}^K$ denotes the importance of all views for sequence i . Finally, we use the weights to combine the latent representations for each view as

$$\tilde{u}_i = \sum_{j=1}^K \alpha_i^{(j)} u_i^{(j)}. \quad (6)$$

Thus, \tilde{u}_i , called the *combined view embedding* represents combined knowledge from correlations learned by all views weighted by their importance for final prediction distribution. We denote the set of *combined view embeddings* for all sequences as $\mathcal{U} = \{\tilde{u}_i\}_{i=1}^N$.

4.4 Forecast Distribution Decoder

Having extracted stochastic representations from each of the views leveraging latent encoders, VSCGs and the View selection module, we learn the output distribution via the *Decoder module*. The decoder module uses the combined view embeddings \mathcal{U} and the sequence embedding of default view $\mathcal{Z}^{X,(1)}$ to learn the parameters of output distribution. While \mathcal{U} directly uses only the selectively aggregated embeddings of reference sets, $\mathcal{Z}^{X,(1)}$ leverages local historical patterns of input sequence including novel information that can be used to extrapolate beyond information from reference sets of multiple views. The final decoder process is described as:

$$\begin{aligned} e_i &= z_i^{(1)} \oplus \tilde{u}_i \\ \mu(y_i), \sigma(y_i) &= d_1(e_i), \exp(d_2(e_i)) \\ \hat{y}_i^{(t+\tau)} &\sim \mathcal{N}(\mu(y_i), \sigma(y_i)), \end{aligned} \quad (7)$$

where d_1 and d_2 and feed-forward layers and \oplus is the concatenation operator. Here, we used a multivariate Gaussian distribution to parameterize $P(y_i^{(t+\tau)} | e_i)$ since our target sequence has real numbers. However, this framework can be extended to discrete and integer-valued output by carefully choosing the appropriate distribution and their relevant statistic to predict.

4.5 Model Training and Inference

The generative process of CAMUL can be summarized as

$$\begin{aligned} P(\{y_i^{t+\tau}\}_{i=1}^N | \mathcal{X}, \mathcal{R}) &= \int \underbrace{\sum_{j=1}^K [P(\mathcal{Z}^{X,(j)} | \mathcal{X}^{(j)}) P(\mathcal{Z}^{R,(j)} | \mathcal{R}^{(j)})]}_{\text{Stochastic latent encoders}} \\ &\underbrace{P(G^{(j)} | \mathcal{Z}^{X,(j)}, \mathcal{Z}^{R,(j)}) P(\mathcal{U}^{(j)} | G^{(j)})}_{\text{VSCG}} \\ &\underbrace{P(\mathcal{U} | \{\mathcal{U}^{(j)}\}_{j=1}^K)}_{\text{View selection}} \underbrace{P(\{y_i^{t+\tau}\}_{i=1}^N | \mathcal{U}, \mathcal{Z}^{X,(1)})}_{\text{Output distribution}} d\{\mathcal{Z}^{(j)}\}_j d\mathcal{U}. \end{aligned}$$

Our objective is to increase the log-likelihood of above equation which is intractable due to integrals over real-valued random variables. Therefore, we use variational inference by approximating the posterior $\prod_{j=1}^K P(\mathcal{Z}^{(j)}, \mathcal{U}^{(j)}, G^{(j)} | \mathcal{X}^{(j)}, \mathcal{R}^{(j)}) P(\mathcal{U} | \{\mathcal{U}^{(j)}\}_j)$ with the variational distribution :

$$q_j(\mathcal{U}^{(j)}, \mathcal{Z}^{(j)}, G^{(j)} | \mathcal{X}^{(j)}) = P(\mathcal{Z}^{X,(j)} | \mathcal{X}^{(j)}) P(\mathcal{Z}^{R,(j)} | \mathcal{R}^{(j)}) P(G^{(j)} | \mathcal{Z}^{X,(j)}, \mathcal{Z}^{R,(j)}) q_j(\mathcal{U}^{(j)} | \mathcal{X}^{(1)}),$$

for each view j , where q_j is a 2-layer network that parametrizes the Gaussian distribution $q_j(\mathcal{U}^{(j)} | \mathcal{X}^{(1)})$ with input sequences $\mathcal{X}^{(1)}$. The ELBO is derived to be:

$$\mathcal{L} = -E_{q_j(\mathcal{Z}^{(j)}, G^{(j)}, \mathcal{U}^{(j)} | \mathcal{X}^{(j)})} [\log P(\{y_i^{t+\tau}\}_{i=1}^N | \mathcal{U}, \mathcal{Z}^{X,(1)}) + \sum_{j=1}^K \log P(\mathcal{U}^{(j)} | G^{(j)}, \mathcal{Z}^{(j)}) - \log q_j(\mathcal{U}^{(j)} | \mathcal{X}^{(1)})].$$

The parameters of the inference distributions q_j and the components of the generative process are jointly learned via Stochastic Gradient Variational Bayes to minimize the ELBO loss (Kingma and Welling 2013). We use the reparametrization trick for all sampling processes. During inference, we sample from the joint distribution $P(\{y_i^{t+\tau}\}_{i=1}^N, \{\mathcal{Z}^{(j)}, G^{(j)}\}_j, \mathcal{U} | \mathcal{X}, \mathcal{R})$ to generate samples for the forecast distribution $\{y_i^{t+\tau}\}_{i=1}^N$. The pseudo-code for training and inference is available in Appendix.

5 Experiments

We evaluated our models on a workstation that runs on Intel Xeon 64 core processor with 128 GB memory on a single Nvidia Tesla V100 GPU. Our model takes less than 6 GB of memory and typically takes 20-40 minutes of training time for each of the benchmarks discussed below. We describe the baselines, benchmark datasets and tasks as well as evaluation metrics with additional details in the Appendix.

Baselines: We compare our model against the state-of-art probabilistic forecasting baselines along with some domain-specific baselines. The chosen forecasting baselines have shown state-of-art performance on a wide set of probabilistic forecasting tasks such as power consumption, air quality, traffic forecasting, health risk assessment, data center load estimation, etc. **SARIMA** (Hyndman and Athanasopoulos 2018): A classic time-series forecasting baseline based on ARIMA that accounts for seasonal shifts. **DeepAR** (Salinas et al. 2020): A state-of-art, widely used RNN based probabilistic forecasting model that learns a parametric distribution. **Deep State Space Model (DSSM)** (Li et al. 2021): A space state based model that uses neural networks to model transition and emission distribution of state space. **Deep Graph Factors (GraphDF)** (Chen et al. 2021b): A deep probabilistic forecasting model that integrates relational information from graphs across time-series. In absence of explicit relational information, Chen et al. (2021b) proposes to use RBF kernel over the euclidean distance as edge weights over pairs of time-series, which we use as the **GraphDF-RBF** baseline. If explicit relational data in form of adjacency graph

is available (in case of all benchmarks except `power`), we also evaluate using this adjacency graph as the **GraphDF-Adj** baseline. **Recurrent neural process (RNP)** (Qin et al. 2019): Neural Process based method for temporal data which uses attention over reference points as part of the generative process. **Multi-modal Gaussian Process (MMGP)**: Similar to (Chen et al. 2021a) we first pre-train a deterministic model combining deterministic embeddings from the encoders and aggregating embeddings with fixed learned weights to predict the output. Then we aggregate the embeddings as features to train a Gaussian Process to get probabilistic predictions.

For disease forecasting benchmarks, we also evaluate against state-of-art domain-specific forecasting models that use the same set of exogenous features as described in Table 1. We choose top performing deep learning models for flu-forecasting `google-symptoms` task: EpiDeep (Adhikari et al. 2019) and EpiFNP (Kamarthi et al. 2021). For the `covid19` task, we also choose CMU-TS (Cramer et al. 2021) and DeepCovid (Rodríguez et al. 2021b) as baselines; these leverage the CovDS dataset and are the best statistical models at the Covid-19 Forecast Hub organized by CDC (Cramer et al. 2021). We also evaluate against variants of CAMUL which enable us to examine the importance of Context-Specific View Selection and probabilistic view-specific modeling (see Q2 of Results).

Benchmarks: We evaluate CAMUL framework on time-series forecasting problem from a variety of domains involving diverse types of data views as described in Table 1.

Evaluation metrics: We evaluate our model and baselines using probabilistic metrics that test for both accuracy and calibration of forecasts. We use the Cumulative ranked probability score (CRPS), a standard probabilistic metric (Gneiting and Katzfuss 2014). Interval Score (IS), which is a popular probabilistic forecast metric in epidemic forecasting (Reich et al. 2019), is also used. In order to measure calibration of forecasts, we use the Calibration Score (CS) based on (Kamarthi et al. 2021; Kuleshov, Fenner, and Ermon 2018).

5.1 Results

Q1: *Does CAMUL provide well-calibrated accurate probabilistic forecasts across all benchmarks?*

We evaluate our model and baselines on the four tasks described in the experiment section above. We ran the experiments 20 times for each of the models for all tasks and reported the mean scores. The results are summarized in Tables 2. For `covid19` and `google-symptoms`, we show 2-week ahead results here and rest, which show similar trends, in Appendix. CAMUL models significantly outperform the baselines in all the probabilistic and calibration scores. Specifically for the hard disease-forecasting tasks we see over 25% improvement in CRPS score and 50% improvement in interval score over best baselines. In case of `power` and `tweet`, we observe 28% and 24% improvement in CRPS scores over second-best model and 56% and 35% improvement in interval score. Performing significance test (t-test) with $\alpha = 1\%$ shows that CAMUL is significantly better than other models in all scores except those highlighted in bold in Table 2. Applying post-hoc calibration methods (Kuleshov, Fenner, and

| Benchmark | Dataset | Target | Views(View type) |
|------------------------------------|--|--|---|
| google-symptoms (Health 2021) | Historical wILI sequences and anonymized search volumes for 14 flu-related symptoms for 10 HHS regions and national level. | Future wILI values for each HHS region’s sequence at 1- to 4-weeks ahead | Past sequences (Sequence) HHS adjacency (Graph) Months (Static) |
| covid19 (Cramer et al. 2021) | Weekly data related to Covid-19 surveillance including from hospital records, mortality, hospitalization counts, mobility, exposure and survey data collected by (Kamarthi et al. 2021) for 50 US states | Mortality for 50 US states at 1- to 4-weeks ahead | Mortality (Sequence) Line-list (Sequence) Mobility (Sequence) Demographics (Static) State adjacency (Graph) |
| power (Hebrail and Berard 2012) | Minute-wise Household power consumption measurements for a year with a total of 260,640 measurements each with 7 features from 3 meters. | Total active power consumption next minute | Past sequence (Sequence) Time-of-day (Static) Month (Static) |
| tweet (Shi et al. 2019) | Weekly Tweet topic distribution for tweets related to Covid-19 pandemic with topics extracted using LDA. | 1-week ahead topic distribution | Past sequence (Sequence) State adjacency (Graph) Month (Static) Demographics (Static) |

Table 1: Description of benchmark tasks: datasets, target and views.

| | power | | | | tweet | | |
|-------------|--------------------|---------------------|---------------------|-------------|---------------------|---------------------|--------------------|
| | CRPS | CS | IS | | CRPS | CS | IS |
| SARIMA | 1.16 ± 0.018 | 0.23 ± 0.002 | 3.49 ± 0.021 | SARIMA | 1.41 ± 0.262 | 0.37 ± 0.007 | 3.87 ± 0.74 |
| DeepAR | 0.72 ± 0.002 | 0.04 ± 0.003 | 1.57 ± 0.046 | DeepAR | 1.06 ± 0.152 | 0.15 ± 0.003 | 1.35 ± 0.31 |
| DSSM | 0.59 ± 0.018 | 0.02 ± 0.002 | 1.32 ± 0.054 | DSSM | 0.92 ± 0.173 | 0.07 ± 0.002 | 0.96 ± 0.34 |
| RNP | 0.85 ± 0.015 | 0.19 ± 0.005 | 3.31 ± 0.018 | RNP | 1.16 ± 0.045 | 0.22 ± 0.006 | 3.05 ± 0.52 |
| MMGP | 1.19 ± 0.041 | 0.15 ± 0.001 | 3.03 ± 0.013 | MMGP | 1.31 ± 0.162 | 0.13 ± 0.0026 | 1.65 ± 0.49 |
| GraphDF-RBF | 0.92 ± 0.03 | 0.13 ± 0.004 | 1.45 ± 0.033 | GraphDF-RBF | 0.62 ± 0.052 | 0.08 ± 0.010 | 1.91 ± 0.76 |
| | | | | GraphDF-Adj | 0.91 ± 0.031 | 0.14 ± 0.009 | 2.39 ± 0.26 |
| CAMUL | 0.46 ± 0.02 | 0.02 ± 0.001 | 0.93 ± 0.021 | CAMUL | 0.42 ± 0.015 | 0.05 ± 0.004 | 0.68 ± 0.21 |
| CAMUL-C | 1.13 ± 0.04 | 0.08 ± 0.001 | 2.88 ± 0.014 | CAMUL-C | 0.84 ± 0.0027 | 0.07 ± 0.002 | 1.03 ± 0.17 |
| CAMUL-S | 0.68 ± 0.05 | 0.04 ± 0.002 | 1.27 ± 0.027 | CAMUL-S | 0.58 ± 0.081 | 0.05 ± 0.006 | 1.41 ± 0.25 |
| CAMUL-D | 1.36 ± 0.07 | 0.14 ± 0.001 | 2.96 ± 0.012 | CAMUL-D | 1.15 ± 0.020 | 0.19 ± 0.001 | 1.14 ± 0.15 |

| | covid19 | | | | google-symptoms | | |
|-------------|--------------------|---------------------|---------------------|-------------|---------------------|---------------------|---------------------|
| | CRPS | CS | IS | | CRPS | CS | IS |
| SARIMA | 61 ± 3.40 | 0.42 ± 0.017 | 6.32 ± 0.042 | SARIMA | 1.14 ± 0.017 | 0.43 ± 0.008 | 3.11 ± 0.240 |
| DeepAR | 32.6 ± 6.40 | 0.19 ± 0.015 | 2.21 ± 0.015 | DeepAR | 0.55 ± 0.013 | 0.14 ± 0.003 | 1.42 ± 0.130 |
| DSSM | 49.6 ± 3.10 | 0.22 ± 0.009 | 2.13 ± 0.041 | DSSM | 0.52 ± 0.011 | 0.13 ± 0.003 | 2.11 ± 0.140 |
| RNP | 51.2 ± 7.60 | 0.35 ± 0.018 | 4.33 ± 0.031 | RNP | 0.71 ± 0.047 | 0.43 ± 0.006 | 4.13 ± 0.150 |
| MMGP | 25.2 ± 1.10 | 0.27 ± 0.012 | 3.19 ± 0.015 | MMGP | 0.68 ± 0.021 | 0.21 ± 0.008 | 1.87 ± 0.410 |
| GraphDF-RBF | 31.4 ± 2.80 | 0.21 ± 0.017 | 2.75 ± 0.046 | GraphDF-RBF | 0.59 ± 0.016 | 0.08 ± 0.002 | 1.03 ± 0.240 |
| GraphDF-Adj | 37.6 ± 3.30 | 0.28 ± 0.013 | 2.44 ± 0.017 | GraphDF-Adj | 0.64 ± 0.057 | 0.08 ± 0.005 | 2.87 ± 0.610 |
| DeepCovid | 30.5 ± 7.10 | 0.18 ± 0.011 | 3.41 ± 0.029 | EpiDeep | 0.93 ± 0.046 | 0.24 ± 0.007 | 4.26 ± 0.910 |
| CMU-TS | 21.8 ± 4.80 | 0.14 ± 0.015 | 3.17 ± 0.064 | EpiFNP | 0.31 ± 0.051 | 0.04 ± 0.002 | 0.56 ± 0.180 |
| CAMUL | 17.4 ± 5.40 | 0.15 ± 0.007 | 1.42 ± 0.017 | CAMUL | 0.24 ± 0.060 | 0.04 ± 0.004 | 0.43 ± 0.020 |
| CAMUL-C | 18 ± 3.10 | 0.19 ± 0.003 | 1.73 ± 0.024 | CAMUL-C | 0.29 ± 0.022 | 0.05 ± 0.001 | 0.48 ± 0.060 |
| CAMUL-S | 18.4 ± 2.90 | 0.15 ± 0.007 | 1.64 ± 0.037 | CAMUL-S | 0.31 ± 0.064 | 0.04 ± 0.006 | 0.46 ± 0.020 |
| CAMUL-D | 27.3 ± 7.10 | 0.31 ± 0.012 | 3.26 ± 0.021 | CAMUL-D | 0.74 ± 0.081 | 0.19 ± 0.002 | 1.83 ± 0.040 |

Table 2: Evaluation scores (over 20 runs) for CAMUL and baselines for all benchmarks. The best performing scores are shown in bold. We performed t-test with $\alpha = 1\%$. The score in bold are statistically significantly better than other models.

Ermon 2018; Song et al. 2019) on baselines also does not affect the significance of our results (Table 5 in Appendix).

Q2 : Effect of multi-source stochastic modelling and context-sensitive dynamic view selection on CAMUL’s performance

We evaluate the efficacy of Context-Specific Dynamic Views Selection and probabilistic modeling of each data view via Multi-view Latent Probabilistic Encoders and VSCG. We compare the attention based dynamic view selection of CAMUL with two other variants a) **CAMUL-C** concatenates SVCG-based latent embeddings from all views, b) **CAMUL-S** learns a static weight $w^{(j)}$ for each view j and combines the VSCG-based embeddings: $\tilde{u}_i = \sum_j w^{(j)} u_i^{(j)}$, c) To test

the efficacy of stochastic modelling of latent embeddings, the variant **CAMUL-D** uses *deterministic* view-specific latent variables: We use the latent encoders’ mean rather than sampling from Gaussian as Eqn. 1 and use a cross-attention layer over reference points instead of VSCG to derive the view specific latent variables as a weighted summation of reference points. The evaluation scores of the variants are shown in Table 2. We see that the original configuration of CAMUL with dynamic view selection and multi-source probabilistic modeling provides the best scores. Using deterministic multi-source latent embeddings, in particular, drastically decreases the scores showing the efficacy of uncertainty modeling.

Q3: Does CAMUL handle information and uncertainty from multiple views to provide better performance?

| | power | tweet | covid19 | google-symptoms |
|----------------|-------------|-------------|-------------|-----------------|
| All Views | 0.46 | 0.42 | 17.4 | 0.24 |
| Default view | 1.03 | 0.95 | 24.3 | 0.39 |
| Two Best Views | 0.63 | 0.77 | 18.3 | 0.35 |
| Best Baseline | 0.59 | 0.62 | 21.8 | 0.31 |

Table 3: Comparison of CRPS score of CAMUL with all views, default view 1, 2 best views and best baseline.

CAMUL models useful patterns and uncertainty for each of the diverse set of data views independently before combining them. This is in contrast to most baselines that use simple aggregation at feature level or latent embedding level where noisy or reliable data from some views may hinder performance. CAMUL however learns to weigh the importance of each view before combining them for prediction. To test the efficacy of CAMUL’s handling of multiple data views, we evaluated the model with a single default view, two best views and compared it with the original CAMUL with all views and the best performing baseline as shown in Table 3. Note that for all benchmarks, the best view is always the default view. We see that model with all views is clearly the best performing. Moreover, using only the best view sometimes leads to lower performance compared to the best performing baseline which has access to data from all views. Therefore, we conclude that CAMUL can handle multiple views that in turn lead to significantly better performance..

Q4: Does weights of each view from View Selection module correspond to predictive utility of the view?

The attention weights learned by the view selection module in Eqn. 5 informs the learned importance of views that are used for aggregating view-aware latent embeddings. We observed that the default view 1 containing time-series sequences was almost always the most highly weighted views and was necessary for model to perform reasonably. Next, we study the correlation between attention weights and the efficacy of other views and the efficacy of the views. We assess the efficacy of a view by training variant of CAMUL with two views: the default view and view we are interested in. We compare the CRPS scores of these variants to the attention weights and see that the CRPS scores are inversely proportional to the view selection module weight (See above Figure for an example for covid19 task). This further shows that the view selection module, indeed, selects the most informative views on average to improve the performance of our CAMUL models.

Q5: Does the dynamic view-selection module adapt across time to select informative views?

We provide specific case-studies to show the efficacy of the view selection module in selecting useful views specific to the input sequence by studying the attention weights. We describe a case-study related to covid19 below and one related to google-symptoms in the Appendix.

Obs 1: For the covid19 task, weights of mobility view are higher than default sequence view during early pandemic (June and July) for many highly populous US states.

| State | Month | Seq. | Line-list | Mobility | Adj. | Demo. |
|-------|-------|------|-----------|----------|------|-------|
| TX | June | 0.32 | 0.22 | 0.37 | 0.03 | 0.06 |
| | July | 0.37 | 0.23 | 0.31 | 0.05 | 0.04 |
| GA | June | 0.21 | 0.34 | 0.31 | 0.01 | 0.13 |
| | July | 0.24 | 0.40 | 0.26 | 0.02 | 0.08 |
| MA | June | 0.32 | 0.19 | 0.36 | 0.04 | 0.09 |
| | July | 0.39 | 0.29 | 0.23 | 0.02 | 0.07 |
| NY | June | 0.25 | 0.24 | 0.32 | 0.04 | 0.15 |
| | July | 0.26 | 0.34 | 0.27 | 0.01 | 0.12 |

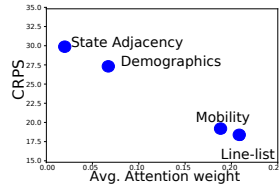
Table 4: Avg. Attention weight of View selection module during June and July for some populous US states.

The average attention weight on the default view is over 40% for all months over all states. However, during the initial 2 months of the dataset (June and July), 12 states observed higher weight for mobility view including populous states such as TX, GA, MA and NY. We found that CAMUL’s view selection module adapted by relying more on the mobility view data during the initial months for mortality forecasting. This concurs with studies that at the initial stages of the pandemic, decrease in mobility was highly correlated with decrease in the disease spread (Chang et al. 2021), but later on, this changed (Rodríguez et al. 2021b). In addition, line-list data was error-prone during the initial months of the pandemic because the reporting systems were not yet in place (Rodríguez et al. 2021a) whereas the mobility features extracted from digital sources were more accurate in real-time (Budd et al. 2020).

6 Conclusion

We introduced CAMUL, a general non-parametric generative framework for multi-source, multi-modal probabilistic forecasting. Our framework successfully tackles the challenge of modeling probabilistic information and uncertainty from diverse data views of multiple modalities across multiple domain benchmarks. CAMUL outperformed both state-of-art general probabilistic baselines as well as top domain-specific baselines, resulting in over 25% improvement in accuracy and calibration metrics. Our case-studies also empirically showed the importance of joint probabilistic modeling and context-sensitive integration from multiple views. It automatically adapts to select more useful data views as seen in the covid19 and google-symptoms case studies.

CAMUL can easily be applied to any multi-source and multi-modal forecasting task by using appropriate encoders to encode a variety of data where capturing multi-source uncertainty is important. Analysis of view selection for specific tasks can also help understand data reliability, the disparity in data quality across sensitive parameters. As future work, our work can also be extended to tasks such as anomaly detection, change point detection and time-series segmentation where drastic variation in confidence intervals and view selection weights can be a useful predictive indicator of important behaviors.



References

- Adhikari, B.; Xu, X.; Ramakrishnan, N.; and Prakash, B. A. 2019. Epideep: Exploiting embeddings for epidemic forecasting. In *Proceedings of the 25th ACM SIGKDD International Conference on Knowledge Discovery & Data Mining*, 577–586.
- Blei, D. M.; Ng, A. Y.; and Jordan, M. I. 2003. Latent dirichlet allocation. *the Journal of machine Learning research*, 3: 993–1022.
- Budd, J.; Miller, B. S.; Manning, E. M.; Lampos, V.; Zhuang, M.; Edelstein, M.; Rees, G.; Emery, V. C.; Stevens, M. M.; Keegan, N.; et al. 2020. Digital technologies in the public-health response to COVID-19. *Nature medicine*, 26(8): 1183–1192.
- Centers for Disease Control and Prevention, U. 2021. Flu Symptoms & Complications.
- Chang, S.; Pierson, E.; Koh, P. W.; Gerardin, J.; Redbird, B.; Grusky, D.; and Leskovec, J. 2021. Mobility network models of COVID-19 explain inequities and inform reopening. *Nature*, 589(7840): 82–87.
- Chen, C.; Liang, J.; Ma, F.; Glass, L.; Sun, J.; and Xiao, C. 2021a. UNITE: Uncertainty-based Health Risk Prediction Leveraging Multi-sourced Data. In *Proceedings of the Web Conference 2021*, 217–226.
- Chen, H.; Rossi, R. A.; Mahadik, K.; Kim, S.; and Eldardiry, H. 2021b. Graph Deep Factors for Forecasting with Applications to Cloud Resource Allocation. In *Proceedings of the 27th ACM SIGKDD Conference on Knowledge Discovery & Data Mining*, 106–116.
- Cho, K.; Van Merriënboer, B.; Gulcehre, C.; Bahdanau, D.; Bougares, F.; Schwenk, H.; and Bengio, Y. 2014. Learning phrase representations using RNN encoder-decoder for statistical machine translation. *arXiv preprint arXiv:1406.1078*.
- Chung, J.; Kastner, K.; Dinh, L.; Goel, K.; Courville, A. C.; and Bengio, Y. 2015. A recurrent latent variable model for sequential data. *Advances in neural information processing systems*, 28: 2980–2988.
- Cramer, E. Y.; Lopez, V. K.; Niemi, J.; George, G. E.; Cegan, J. C.; Dettwiller, I. D.; England, W. P.; Farthing, M. W.; Hunter, R. H.; Lafferty, B.; et al. 2021. Evaluation of individual and ensemble probabilistic forecasts of COVID-19 mortality in the US. *medRxiv*.
- Ekambaram, V.; Manglik, K.; Mukherjee, S.; Sajja, S. S. K.; Dwivedi, S.; and Raykar, V. 2020. Attention based Multi-Modal New Product Sales Time-series Forecasting. In *Proceedings of the 26th ACM SIGKDD International Conference on Knowledge Discovery & Data Mining*, 3110–3118.
- Fraccaro, M.; Sønderby, S. K.; Paquet, U.; and Winther, O. 2016. Sequential neural models with stochastic layers. *Advances in neural information processing systems*.
- Garnelo, M.; Schwarz, J.; Rosenbaum, D.; Viola, F.; Rezende, D. J.; Eslami, S.; and Teh, Y. W. 2018. Neural processes. *arXiv preprint arXiv:1807.01622*.
- Gneiting, T.; and Katzfuss, M. 2014. Probabilistic forecasting. *Annual Review of Statistics and Its Application*, 1: 125–151.
- Hamilton, W. L. 2020. Graph representation learning. *Synthesis Lectures on Artificial Intelligence and Machine Learning*, 14(3): 1–159.
- Health, G. 2021. Using symptoms search trends to inform COVID-19 research.
- Hebrail, G.; and Berard, A. 2012. Individual household electric power consumption Data Set. *UCI Machine Learning Repository*.
- Hu, W.; Yang, Y.; Wang, J.; Huang, X.; and Cheng, Z. 2020. Understanding electricity-theft behavior via multi-source data. In *Proceedings of The Web Conference 2020*, 2264–2274.
- Hyndman, R. J.; and Athanasopoulos, G. 2018. *Forecasting: principles and practice*. OTexts.
- Jang, E.; Gu, S.; and Poole, B. 2017. Categorical reparameterization with gumbel-softmax. *ICLR*.
- Kamarthi, H.; Kong, L.; Rodríguez, A.; Zhang, C.; and Prakash, B. A. 2021. When in Doubt: Neural Non-Parametric Uncertainty Quantification for Epidemic Forecasting. *arXiv preprint arXiv:2106.03904*.
- Kamarthi et al., H. 2021. Back2Future: Leveraging Backfill Dynamics for Improving Real-time Predictions in Future. *arXiv preprint arXiv:2106.04420*.
- Kingma, D. P.; and Ba, J. 2014. Adam: A method for stochastic optimization. *arXiv preprint arXiv:1412.6980*.
- Kingma, D. P.; and Welling, M. 2013. Auto-encoding variational bayes. *arXiv preprint arXiv:1312.6114*.
- Kipf, T.; and Welling, M. 2016. Semi-Supervised Classification with Graph Convolutional Networks. *ICLR*.
- Krishnan, R.; Shalit, U.; and Sontag, D. 2017. Structured inference networks for nonlinear state space models. In *Proceedings of the AAAI Conference on Artificial Intelligence*, volume 31.
- Kuleshov, V.; Fenner, N.; and Ermon, S. 2018. Accurate uncertainties for deep learning using calibrated regression. In *International Conference on Machine Learning*, 2796–2804. PMLR.
- Leon Barrett, A. K., Stephan Hoyer; and O’Kane, D. 2015. *propperscoring 0.1*. The Climate Corporation.
- Leskovec, J.; Rajaraman, A.; and Ullman, J. D. 2020. *Mining of massive data sets*. Cambridge university press.
- Li, L.; Yan, J.; Yang, X.; and Jin, Y. 2021. Learning interpretable deep state space model for probabilistic time series forecasting. *International Joint Conference on Artificial Intelligence*.
- Li, Y.; Hao, Z.; and Lei, H. 2016. Survey of convolutional neural network. *Journal of Computer Applications*, 36(9): 2508–2515.
- Li, Y.; Yang, M.; and Zhang, Z. 2018. A survey of multi-view representation learning. *IEEE transactions on knowledge and data engineering*, 31(10): 1863–1883.
- Lim, B.; and Zohren, S. 2021. Time-series forecasting with deep learning: a survey. *Philosophical Transactions of the Royal Society A*, 379(2194): 20200209.

- Louizos, C.; Shi, X.; Schutte, K.; and Welling, M. 2019. The Functional Neural Process. In Wallach, H.; Larochelle, H.; Beygelzimer, A.; d'Alché-Buc, F.; Fox, E.; and Garnett, R., eds., *Advances in Neural Information Processing Systems*, volume 32. Curran Associates, Inc.
- Qin, S.; Zhu, J.; Qin, J.; Wang, W.; and Zhao, D. 2019. Recurrent attentive neural process for sequential data. *arXiv preprint arXiv:1910.09323*.
- Ramchandani, A.; Fan, C.; and Mostafavi, A. 2020. Deep-covidnet: An interpretable deep learning model for predictive surveillance of covid-19 using heterogeneous features and their interactions. *IEEE Access*, 8: 159915–159930.
- Rangapuram, S. S.; Seeger, M. W.; Gasthaus, J.; Stella, L.; Wang, Y.; and Januschowski, T. 2018. Deep state space models for time series forecasting. *Advances in neural information processing systems*, 31: 7785–7794.
- Reich, N. G.; Brooks, L. C.; Fox, S. J.; Kandula, S.; McGowan, C. J.; Moore, E.; Osthus, D.; Ray, E. L.; Tushar, A.; Yamana, T. K.; et al. 2019. A collaborative multiyear, multimodel assessment of seasonal influenza forecasting in the United States. *Proceedings of the National Academy of Sciences*, 116(8): 3146–3154.
- Rodríguez, A.; Muralidhar, N.; Adhikari, B.; Tabassum, A.; Ramakrishnan, N.; and Prakash, B. A. 2021a. Steering a Historical Disease Forecasting Model Under a Pandemic: Case of Flu and COVID-19. In *Proceedings of the AAAI Conference on Artificial Intelligence*, volume 35, 4855–4863.
- Rodríguez, A.; Tabassum, A.; Cui, J.; Xie, J.; Ho, J.; Agarwal, P.; Adhikari, B.; and Prakash, B. A. 2021b. DeepCOVID: An Operational Deep Learning-driven Framework for Explainable Real-time COVID-19 Forecasting. In *Proceedings of the AAAI Conference on Artificial Intelligence*, volume 35, 15393–15400.
- Salehinejad, H.; Sankar, S.; Barfett, J.; Colak, E.; and Valaee, S. 2017. Recent advances in recurrent neural networks. *arXiv preprint arXiv:1801.01078*.
- Salinas, D.; Flunkert, V.; Gasthaus, J.; and Januschowski, T. 2020. DeepAR: Probabilistic forecasting with autoregressive recurrent networks. *International Journal of Forecasting*, 36(3): 1181–1191.
- Shi, H.; Zhang, C.; Yao, Q.; Li, Y.; Sun, F.; and Jin, D. 2019. State-sharing sparse hidden markov models for personalized sequences. In *Proceedings of the 25th ACM SIGKDD International Conference on Knowledge Discovery & Data Mining*, 1549–1559.
- Song, H.; Diethe, T.; Kull, M.; and Flach, P. 2019. Distribution calibration for regression. In *International Conference on Machine Learning*, 5897–5906. PMLR.
- Stock, J. H.; and Watson, M. W. 2001. Vector autoregressions. *Journal of Economic perspectives*, 15(4): 101–115.
- Vaswani, A.; Shazeer, N.; Parmar, N.; Uszkoreit, J.; Jones, L.; Gomez, A. N.; Kaiser, Ł.; and Polosukhin, I. 2017. Attention is all you need. In *Advances in neural information processing systems*, 5998–6008.
- Yan, X.; Hu, S.; Mao, Y.; Ye, Y.; and Yu, H. 2021. Deep multi-view learning methods: a review. *Neurocomputing*.
- Zheng, X.; Zaheer, M.; Ahmed, A.; Wang, Y.; Xing, E. P.; and Smola, A. J. 2017. State space LSTM models with particle MCMC inference. *arXiv preprint arXiv:1711.11179*.
- Zhu, L.; and Laptev, N. 2017. Deep and confident prediction for time series at uber. In *2017 IEEE International Conference on Data Mining Workshops (ICDMW)*, 103–110. IEEE.

Appendix for the paper "CAMUL: Calibrated and Accurate Multi-view Time-Series Forecasting"

We provide the code for CAMUL models and anonymized datasets at <https://github.com/AdityaLab/CAMul>.

A Additional Related works

Probabilistic Time-series Forecasting Classical methods of time-series forecasting including exponential smoothing, ARIMA-based models (Hyndman and Athanasopoulos 2018) focus on univariate time-series with small number of exogenous features and learn model parameters independently for each sequence. Vector Auto-regression (VAR) models extend ARIMA based models to multivariate time series (Stock and Watson 2001).

Deep learning based time-series models (Lim and Zohren 2021) such as RNN, GRU and LSTMs, transformers (Vaswani et al. 2017) have proven useful in modelling for large number of features capturing long-range complex non-linear patterns in sequences. However, these methods are trained for point-prediction tasks. DeepAR (Salinas et al. 2020) directly models the mean and variance parameters of the forecast distribution using RNN-based architecture. Some recent works are inspired from the space-state models to explicitly model the transition and emission components with deep learning modules such as in the case of Deep Markov Models (Krishnan, Shalit, and Sontag 2017), and recent Deep State Space models (Li et al. 2021; Rangapuram et al. 2018). Others introduce stochasticity into state dynamics of recurrent neural networks such as Stochastic RNN (Fraccaro et al. 2016), Variational RNN (Chung et al. 2015) and State Space LSTM (Zheng et al. 2017). Bayesian Neural Networks have also been used to model time-series forecast distributions (Zhu and Laptev 2017) but require assigning useful priors to parameters and comes with high computational cost of learning.

Neural Process (NP) (Garnelo et al. 2018) models a global latent variable for entire dataset to capture uncertainty with is used with input data’s embedding to model the distribution parameters. Recurrent neural Process (Qin et al. 2019) leverages NP for sequence data. Functional Neural Process (FNP) captures stochastic correlations between input data and datapoints from training distribution to provide a flexible non-parametric mechanism to model output distribution using related training data points in functional space. EpiFNP (Kamrathi et al. 2021) leveraged this flexible modelling towards sequential data to propose a epidemic forecasting model on univariate sequences for state-of-art calibration and uncertainty. In contrast, our work leverages FNP for uncertainty modelling of each of the individual views and then CAMUL jointly model the total uncertainty by carefully combining distributions from different views towards a well-calibrated final output distribution.

Multi-view time-series forecasting Extracting useful information from multiple data sources and data modalities for enriching prediction models has been a very important machine learning problem with challenges that include noisy data sources, integrating information from multiple sources

and handling different levels of uncertainty and reliability. Recent advances in deep learning architectures has allowed us to extract representations from variety of data sources such as images (Li, Hao, and Lei 2016), sequences (Salehinejad et al. 2017), graphs (Hamilton 2020), etc, and combine these modules’ representation for training in an end-to-end fashion. In order to integrate these methods most methods employ simple summation or concatenation methods (Yan et al. 2021; Li, Yang, and Zhang 2018). For instance DeepCovidNet (Ramchandani, Fan, and Mostafavi 2020) uses spatio-temporal and static features using simple summation for Covid-19 prediction. Ekambaram et al. (2020) similarly integrate images, text and static features for predicting consumer sales.

Moreover, most of these methods do not focus on probabilistic forecasting unlike (Chen et al. 2021a) which uses EHR sequence data, static demographic and location data and learn a data-source specific weight by pre-training the aggregated embeddings on prediction task of deciding if patient requires a treatment. Then, they employ a Gaussian Process approach to learn forecast probability on these embeddings to capture uncertainty.

In contrast, we model data-view specific and modality specific uncertainty by learning a latent distribution for each view which allows the model to reason about data reliability, source specific uncertainty and inherent noise when it integrates uncertainty-aware stochastic representations of all views towards the final forecast distribution.

B Examples of Multi-view Probabilistic Latent Encoders

We provide examples of Probabilistic Latent Encoders for data views of different modalities that are used in the paper. Due to generality of our framework, variety of neural encoders can be used specific to data view and type of task.

Static features: We encode the static features of fixed dimensions of form $R_k^{(j)} \in \mathbf{R}^d$. We employ a feed-forward network to capture the parameters of distribution.

Sequences: To capture the latent embedding of sequence $R_k^{(j)} = \{R[0]_k^{(j)}, R[1]_k^{(j)}, \dots, R[T]_k^{(j)}\}$, such as in the default view, we leverage neural sequence encoders GRU (Cho et al. 2014) as:

$$\{\tilde{z}[t]_k^{(j)}\}_{t=0}^T = GRU(\{R[t]_k^{(j)}\}_{t=0}^T) \quad (8)$$

where $\{\tilde{z}[t]_k^{(j)}\}_{t=0}^T$ are the intermediate states of GRU.

In order to capture capture long-term relations and prevent over-emphasis on last terms of sequence we employ self-attention layer introduced in (Vaswani et al. 2017):

$$\{\alpha[0]_d, \alpha[1]_d, \dots, \alpha[T]_d\} = \text{Self-Atten}(\{\tilde{z}[t]_k^{(j)}\}_{t=0}^T) \\ \mu_k^{(j)}, \sigma_k^{(j)} = g'_j \left(\sum_{t=0}^T \alpha[t]_d z[t]_d^{(j)} \right) \quad (9)$$

where g'_j is a single feed-forward layer.

Graph data: If the data type of view j contain relations, i.e, the reference sets have an inherent graph structure denoted by $(A^{(j)}, F^{(j)})$, where $A^{(j)} \in \mathbf{R}^{N_j \times N_j}$ is the adjacency matrix (potentially with weights) and $F^{(j)} = \{f_i^{(j)}\}_{i=1}^{N_j}$ are feature vectors of fixed dimensions, then we can use a Graph Neural network architecture (Kipf and Welling 2016) to encode the relations in $A^{(j)}$:

$$\{\tilde{z}_i^{(j)}\}_{i=1}^{N_j} = GCN(A^{(j)}, \{f_i^{(j)}\}_{i=1}^{N_j}) \quad (10)$$

Then, we use feed forward layer to derive the distribution parameters:

$$\mu_i^{(j)}, \sigma_i^{(j)} = g'_j(\tilde{z}_i^{(j)}) \quad (11)$$

C Implementation details

We used numpy for data processing and PyTorch for model training and inference. We use the properscoring library (Leon Barrett and O’Kane 2015) to implement the CRPS evaluation.

C.1 Data pre-processing

Scaling values: Since time-series and exogenous features can have wide range of values, we normalize the values of each features with mean 0 and variance 1. We derive the scaling factors for training dataset and apply the transformation to test set during inference.

Chunking time-series for training: The long training sequences are split using the shingling technique (Leskovec, Rajaraman, and Ullman 2020; Li et al. 2021) where we fix a window size $W = 10$ and randomly sample chunks of W size from the full sequence over the interval $[1, t - W - 1]$ and record the τ ahead value as ground truth. Note that the reference set of default view 1 still contains the full length sequence of training set, we only use the split sequence as input for training set.

C.2 Hyperparameters

We describe the hyperparameters for CAMUL for all benchmarks.

Multi-view probabilistic encoders For the feed-forward networks of static view, we used a 3 layer network with 60 hidden units. We also used 60 hidden units for GRU of sequence views and used a bi-directional version of GRU. For graph views, we used a 2-layer GCN network with 60 hidden units. The final layer outputs 120 dimensional vector which we split into mean and variance. We apply exponentiation on the variance vector to make it positive. The latent embeddings $z_i^{(j)}$ for all views thus have dimension of 60.

View specific correlation graph The networks l_j^μ and l_j^σ is a 2 layer feed forward network with 60 hidden units. Thus, the dimension of view-aware latent embedding is 60.

Dynamic view-selection module We pass the view-aware latent embeddings and $z_i^{(1)}$ each through a single 60-hidden unit feed forward layer (h_1, h_2) before computing the cross attention weights. The combined-view embedding \tilde{u}_i is a 60 dimensional vector.

Forecast decoder We use a 3 layer feed forward layer that inputs the latent embedding of sequence $z_i^{(1)}$ and \tilde{u}_i and has 60 hidden units in each hidden layer with final layer outputting 2 scalars $\mu(y_i), \sigma(y_i)$.

Throughout all layers of CAMUL we apply exponentiation to variance vector/scalar to make it positive. We also use ReLU activation for hidden layers unless specified otherwise. We also use ADAM optimizer (Kingma and Ba 2014) for parameter updates.

Note on hyperparameter selection We sampled a validation set containing 10% of randomly selected chunks of sequences from training set. This was used for model hyperparameter tuning. We describe splitting of dataset into training and test set in Section D below for each benchmark.

We found that the performance was not significantly sensitive to model architecture, batch size or learning rate. We searched over the space of $\{30, 60, 120, 250\}$ for hidden units and mostly optimized for faster convergence. We also searched over $\{10, 20, 50, 80\}$ for batch-size and found 20, 20, 10, 50 to be most optimal for *tweet*, *covid19*, *google-symptoms*, *power* respectively. We used 0.0005 as learning rate.

For *power* and *google-symptoms* we observed that CAMUL took less than 700 epochs to converge whereas it took 2000 and 1000 epochs for *covid19* and *tweet*. Regarding seed selection, we initialized random seeds to 0 to 19 for numpy and pytorch for the 20 trials done for each benchmarks and didn’t observe any significant variation in scores.

Algorithm 1: Training Algorithm for CAMUL

Input : Training sequences $\{Y_N\}_{i=1}^N = \{X_i^{(1)}\}_{i=1}^N$,
target labels $\{y[t + \tau]_i\}_{i=1}^N$, view data
sources $\{X_i^{(j)}\}_{i=1}^N$ for each view
 $j \in \{2, \dots, K\}$, reference points $\{R_i^{(j)}\}_{i=1}^{N_j}$
for each view j

- 1 **for** $i \sim \{1, \dots, N\}$ **do**
- 2 **for** $j \in \{1, \dots, K\}$ **do**
 /* Stochastic embeddings from
 latent stochastic encoder
 */
- 3 Sample $z_i^{(j)}$ as Eqn 1 using encoder g_{θ_j} ;
- 4 **for** $R_k^{(j)} \in \mathcal{R}^{(j)}$ **do**
- 5 | Sample $z_k^{(j)}$ using encoder g_{θ_j} ;
- 6 **end**
- 7 /* Sample edges for SVCG */
- 8 **for** $R_k^{(j)} \in \mathcal{R}^{(j)}$ **do**
- 9 | Add (k, i) to $G^{(j)}$ with probability
 | $k(z_k^{(j)}, z_i^{(j)})$;
- 10 **end**
- 11 Derive $\mu(u_i^{(j)}), \sigma(u_i^{(j)})$ from sampled edges
 $\{k : (k, i) \in G^{(j)}\}$ as Eqn 4;
 /* Sample from Variational
 distribution */
- 12 Sample $\hat{u}_i^{(j)}$ from variational distribution q_j ;
- 13 **end**
 /* Aggregate all view-aware
 embeddings using Dynamic
 view-selection module */
- 14 Compute importance weights $\{\alpha_i^{(j)}\}_{j=1}^K$ using
 cross-attention as Eqn 5 from $\{\hat{u}_i^{(j)}\}_{j=1}^K$;
- 15 Compute the combined view embedding
 $\tilde{u}_i^{(j)} = \sum_{j=1}^K \alpha_i^{(j)} \hat{u}_i^{(j)}$;
 /* Final output distribution */
- 16 Derive $\mu(y_i), \sigma(y_i)$ from $z_i^{(1)}$ and $\tilde{u}_i^{(j)}$ via the
 decoder (Eqn 7);
 /* Sample ELBO Loss */
- 17 Compute $\mathcal{L}_1 = \log P(y[t + \tau]_i | \mu(y_i), \sigma(y_i))$;
 Compute
 $\mathcal{L}_2 = \sum_{j=1}^K \log P(\hat{u}_i^{(j)} | \mu(u_i^{(j)}), \sigma(u_i^{(j)})) -$
 $\log q_j(\hat{u}_i^{(j)} | X_i^{(j)})$;
- 18 Accumulate gradient for loss $\mathcal{L} = -(\mathcal{L}_1 + \mathcal{L}_2)$;
- 19 **end**
- 20 Periodically update the weights of all modules of
 CAMUL from accumulated gradients using ADAM;

Algorithm 2: Inference Algorithm for CAMUL

Input : Input sequence $Y_i = X_i^{(1)}$, view data sources
 $X_i^{(j)}$ for each view $j \in \{2, \dots, K\}$,
reference points $\{R_i^{(j)}\}_{i=1}^{N_j}$ for each view j

- 1 **for** $j \in \{1, \dots, K\}$ **do**
 /* Stochastic embeddings from
 latent stochastic encoder */
- 2 Sample $z_i^{(j)}$ as Eqn 1 using encoder g_{θ_j} ;
- 3 **for** $R_k^{(j)} \in \mathcal{R}^{(j)}$ **do**
- 4 | Sample $z_k^{(j)}$ using encoder g_{θ_j} ;
- 5 **end**
- 6 /* Sample edges for SVCG */
- 7 **for** $R_k^{(j)} \in \mathcal{R}^{(j)}$ **do**
- 8 | Add (k, i) to $G^{(j)}$ with probability
 | $k(z_k^{(j)}, z_i^{(j)})$;
- 9 **end**
- 10 Sample view-aware latent embedding $u_i^{(j)}$ from
 sampled edges $\{k : (k, i) \in G^{(j)}\}$ as Eqn 4;
- 11 **end**
 /* Aggregate all view-aware
 embeddings using Dynamic
 view-selection module */
- 12 Compute importance weights $\{\alpha_i^{(j)}\}_{j=1}^K$ using
 cross-attention as Eqn 5;
- 13 Compute the combined view embedding
 $\tilde{u}_i^{(j)} = \sum_{j=1}^K \alpha_i^{(j)} u_i^{(j)}$;
 /* Final output distribution */
- 14 Sample $y[t + \tau]_i$ from $z_i^{(1)}$ and $\tilde{u}_i^{(j)}$ via the decoder
 (Eqn 7);

D Details of Benchmarks

google-symptoms: Flu forecasting from Google symptoms We use aggregated and anonymized search counts of flu-related symptoms searches from each US state to predict future incidence of influenza. Dataset: The flu incidence rate is represented by wILI (weighted Influenza related illness) values released weekly by CDC for 8 regions of USA. The aggregate symptom counts for over 400 symptoms are anonymized and publicly released for each week since 2017 at county and state level by Google (Health 2021). We choose to extract 14 symptoms related to influenza referred to in the CDC website (Centers for Disease Control and Prevention 2021). We aggregate these counts for each HHS region and use it as exogenous features. We also use spatial adjacency data between HHS regions and time-related data (month and year) as features. For forecasting wILI values for a given year, we use the training set from all past years for model training and hyperparameter tuning.

Views: We use following diverse views for this benchmarks: 1. *Default Historical wILI view:* This view contains reference points of symptoms features for all previous forecasting seasons for all HHS regions. We use the GRU encoder for this view. 2. *HHS adjacency view:* This is a graph feature view. We have 8 reference points corresponding to HHS regions. The features $\mathcal{F}^{(j)}$ are one-hot encodings. The adjacency matrix $A^{(j)}$ encodes the neighbourhood information between HHS regions that share a border. We aptly use the GCN based latent encoder. 3. *Month view:* This is a static feature view. We have 12 reference points for each month. We use an embedding layer to learn encodings for each reference point from one-hot embedding and use the feed-forward latent encoder.

covid19: Covid-19 mortality forecasting We also evaluate our model on the challenging task of forecasting COVID-19 mortality for each of the 50 US states. Dataset: We use the mortality data and exogenous features used in (Rodríguez et al. 2021b; Kamarthi et al. 2021). The exogenous features contain multiple kinds of data including hospital records, mobility, exposure and survey data. We evaluate for duration of 7 months from June 2020 to December 2020 and again use only past weeks’ data to train before forecasting for 1 to 4 weeks ahead mortality. We train the model separately for each week over all states using data upto past week as training set.

Views: 1. *Default Mortality view:* This is a sequence view where each reference point is a time-series of past mortality. 2. *Line-list view* This is a multivariate sequence view that contains 7 weekly-collected features from traditional surveillance including hospitalization and testing. 3. *Mobility and exposure view* Similarly we use the digitally collected signals measuring aggregate mobility and individuals collected from smartphones. For views 1,2 and 3 we use a GRU based encoder. 4. *Demographic view* This is a static view where we encode each of the 50 states using 8 demographic features including average income, unemployment, population, average age and voting preferences. We use a feed-forward network for encoder. 5. *State adjacency view:* Similar to flu-symptoms we construct a graph view of 50 states

and encode spatial adjacency states. We use a GCN-based encoder.

power :Power consumption forecasting We also evaluate on household power consumption data used as a standard forecasting benchmark. (Hebrail and Berard 2012) Dataset: It contains 260,640 measurements of power consumption of a household for a year using measurements from 3 meters with a total of 7 features. Our goal is to forecast the total active power consumption for 1 minute in future. We use the data from the first 9 months of measurement as training set and last 3 months as test set for forecasting. Views: 1. *Default Past sequence view* We randomly sample single day sequence from each of the past months as reference sets. 2. *Time of Day view:* This is a static view We divide the 24 hours of a day into 6 equal intervals and assign each reference point an interval using one-hot encoding. 3. *Month view:* This is a static view. We assign a reference point for each month using one-hot encodings.

tweet: Tweet Topics prediction Our goal for this task is to evaluate the topic distribution of tweets in the future given topic distributions of past weeks similar to Shi et al. (2019). Dataset: We collect Covid-19 related tweets for 15 weeks that have a geographical tag to identify US state of the user. We extract 30 topics using LDA (Blei, Ng, and Jordan 2003). We also allocate each tweet from a given week to each of the 30 topics it is most likely related to using the LDA model for each state. Thus, we have a multivariate sequence dataset where for each of the 50 states, we have sequences containing topic distribution of tweets for each week. Similar to google-symptoms, for each forecasting for each year, we use data from past year as training set.

Views: 1. *Default Past sequence view:* Similar to other task the first view contains the past sequences for each state. 2. *State adjacency view:* We construct a state adjacency view similar to covid19 task. 3. *Month view:* Similar to power task. 4. *Demographics view* Same as view 4 of covid19 task.

Setup Remarks: We train a separate decoder module for each of the 30 topics. The scores reported are average over all topics.

E Evaluation metrics

Cumulative ranked probability score (CRPS): The CRPS is a standard metric used for evaluation of probabilistic forecasts and is a proper scoring rule that generalizes mean average error to probabilistic forecasting (Gneiting and Katzfuss 2014). Given ground truth y and the predicted probability distribution $\hat{p}(Y)$, let \hat{F}_y be the CDF. Then CRPS is defined as:

$$CRPS(\hat{F}_y, y) = \int_{-\infty}^{\infty} (\hat{F}(\hat{y}) - \mathbf{1}\{\hat{y} > y\})^2 d\hat{y}$$

Interval Score(IS): IS is a standard score used in evaluation of probabilistic forecasts in epidemiology (Reich et al. 2019) which measures the negative log likelihood of a fixed size interval around the ground truth under the predictive distribu-

tion:

$$IS(\hat{p}_y, y) = - \int_{y-L}^{y+L} \log \hat{p}_y(\hat{y}) d\hat{y}.$$

Confidence Score (CS): CS (Kamarthi et al. 2021) measures the overall calibration of predictions of a model M by calculating fraction $k_m(c)$ of prediction distributions that cover the ground truth at each confidence interval c . A perfectly calibrated model has $k_m(c)$ very close to c . We, therefore define CS as:

$$CS(M) = \int_0^1 |k_m(c) - c| dc$$

Calibration score is also similar to Calibration error introduced in Kuleshov, Fenner, and Ermon (2018).

F Correlation between Attention weights of View selection Module and CRPS scores of two view variants

As discussed in Q4 of Section 5.1, the attention weights of the view selection module correlated with the predictive utility of a view which we tested using a 2 view variant of CAMUL containing the default view and the view of interest. The inverse correlation between CRPS and attention weights for all benchmarks is shown in Figure 3.

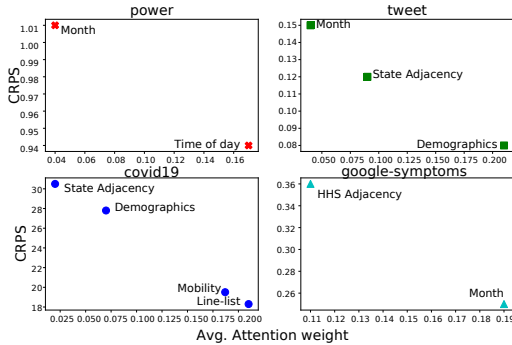


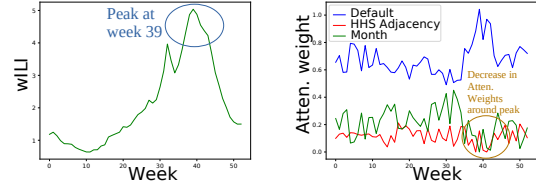
Figure 3: CRPS is inverseley correlated with attention weights of View selection module

G Additional Observation on view selection weights

Obs 2: In relation to google-symptoms task, for the weeks around the peak week, the weights of views other than sequence view decreases by over 30% on average for all HHS regions.

The month and HHS adjacency view capture information about seasonal and average region-specific patterns. However, near the peak weeks where wILI values are more volatile, CAMUL relies on the past wILI sequence patterns including values from past weeks for interpolation which is observed by the sudden decrease in attention weights of other views. Therefore, we observed an average decrease of 32.4% in

attention weights of Month and Adjacency view during the 4 weeks around the peak week (the week with highest wILI value).



(a) wILI values for 2018 sea (b) Average attention weights of views for 2018 season

Figure 4: Sequence view is more important during peak weeks

An example is shown in Figure 4 for the 2018 flu season. We see that the peak week is at week 40. The weights corresponding the past sequence view sees an increase on weeks 38 - 42 whereas weights of other views decrease.

| (a) power | | | | | | |
|-------------|-------------|-------------|-------------|-------------|-------------|-------------|
| Model | Isotonic | | | DC | | |
| | CRPS | CS | IS | CRPS | CS | IS |
| SARIMA | 1.32 | 0.14 | 3.28 | 1.7 | 0.23 | 3.95 |
| DeepAR | 0.67 | 0.04 | 1.55 | 0.71 | 0.08 | 1.64 |
| DSSM | 0.62 | 0.04 | 1.62 | 0.81 | 0.09 | 1.84 |
| RNP | 0.87 | 0.17 | 2.55 | 0.93 | 0.16 | 2.58 |
| GP | 1.03 | 0.12 | 2.78 | 1.03 | 0.12 | 2.78 |
| GraphDF-RBF | 0.92 | 0.13 | 1.45 | 1.04 | 0.18 | 1.31 |
| CAMUL | 0.43 | 0.02 | 0.91 | 0.47 | 0.04 | 1.02 |

| (b) tweet | | | | | | |
|-------------|-------------|-------------|-------------|-------------|-------------|-------------|
| Model | Isotonic | | | DC | | |
| | CRPS | CS | IS | CRPS | CS | IS |
| SARIMA | 1.18 | 0.22 | 3.39 | 1.27 | 0.33 | 3.25 |
| DeepAR | 1.02 | 0.18 | 1.24 | 1.17 | 1.15 | 1.36 |
| DSSM | 1.19 | 0.08 | 1.15 | 1.21 | 0.17 | 1.83 |
| RNP | 1.09 | 0.15 | 1.89 | 1.17 | 0.13 | 2.05 |
| GP | 1.25 | 0.15 | 1.86 | 1.27 | 0.15 | 2.38 |
| GraphDF-RBF | 0.7 | 0.1 | 1.61 | 0.75 | 0.08 | 1.92 |
| GraphDF-Adj | 1.15 | 0.18 | 2.63 | 1.17 | 0.18 | 2.39 |
| CAMUL | 0.55 | 0.06 | 0.68 | 0.67 | 0.07 | 0.86 |

| (c) covid19 | | | | | | |
|-------------|-------------|-------------|-------------|-------------|-------------|-------------|
| Model | Isotonic | | | DC | | |
| | CRPS | CS | IS | CRPS | CS | IS |
| SARIMA | 57.7 | 0.34 | 5.63 | 62.3 | 0.39 | 5.93 |
| DeepAR | 30.4 | 0.16 | 2.11 | 34.2 | 0.21 | 2.23 |
| DSSM | 44.1 | 0.2 | 1.73 | 54 | 0.28 | 2.55 |
| RNP | 39.1 | 0.31 | 3.16 | 39.4 | 0.34 | 4.28 |
| GP | 23.1 | 0.26 | 3.14 | 23.7 | 0.29 | 3.27 |
| GraphDF-RBF | 36 | 0.23 | 2.96 | 36.9 | 0.27 | 2.98 |
| GraphDF-Adj | 38.6 | 0.29 | 2.4 | 38.6 | 0.29 | 2.4 |
| DeepCovid | 29.1 | 0.16 | 2.49 | 29.1 | 0.16 | 2.49 |
| CMU-TS | 21.1 | 0.13 | 2.8 | 21.1 | 0.13 | 2.8 |
| CAMUL | 13.9 | 0.12 | 1.28 | 13.9 | 0.12 | 1.28 |

| (d) google-symptoms | | | | | | |
|---------------------|-------------|-------------|-------------|-------------|-------------|-------------|
| Model | Isotonic | | | DC | | |
| | CRPS | CS | IS | CRPS | CS | IS |
| SARIMA | 0.93 | 0.39 | 2.56 | 0.97 | 0.35 | 2.62 |
| DeepAR | 0.54 | 0.15 | 1.52 | 0.58 | 0.14 | 1.54 |
| DSSM | 0.5 | 0.12 | 2.14 | 0.56 | 0.14 | 2.36 |
| RNP | 0.65 | 0.21 | 2.34 | 0.67 | 0.27 | 1.65 |
| GP | 0.64 | 0.09 | 1.86 | 0.71 | 0.1 | 1.84 |
| GraphDF-RBF | 0.53 | 0.1 | 1.07 | 0.61 | 0.12 | 1.23 |
| GraphDF-Adj | 0.64 | 0.07 | 2.87 | 0.67 | 0.1 | 2.73 |
| EpiDeep | 0.87 | 0.11 | 2.46 | 0.85 | 0.14 | 2.11 |
| EpiFNP | 0.32 | 0.09 | 0.56 | 0.34 | 0.07 | 0.55 |
| CAMUL | 0.25 | 0.05 | 0.41 | 0.23 | 0.06 | 0.47 |

Table 5: Evaluation scores of CAMUL and baselines after applying post-hoc calibration. We use Isotonic regression (Kuleshov, Fenner, and Ermon 2018) and Distribution calibration (Song et al. 2019) methods. The evaluation scores of CAMUL is statistically significantly better and does not change much due to post-hoc methods, implying that our approach produces well-calibrated forecasts without need for such post-hoc correction methods.

| | covid19 (1 week ahead) | | | google-symptoms (1 week ahead) | | | |
|-------------|------------------------|---------------------|---------------------|--------------------------------|---------------------|---------------------|--------------------|
| | CRPS | CS | IS | CRPS | CS | IS | |
| SARIMA | 55 ± 3.7 | 0.36 ± 0.014 | 5.51 ± 0.034 | SARIMA | 1.08 ± 0.017 | 0.38 ± 0.008 | 2.84 ± 0.24 |
| DeepAR | 34.6 ± 5.3 | 0.17 ± 0.018 | 1.97 ± 0.039 | DeepAR | 0.49 ± 0.013 | 0.16 ± 0.003 | 1.11 ± 0.11 |
| DSSM | 45.6 ± 2.1 | 0.15 ± 0.028 | 2.14 ± 0.061 | DSSM | 0.51 ± 0.010 | 0.19 ± 0.003 | 1.53 ± 0.14 |
| RNP | 46.4 ± 6.6 | 0.27 ± 0.013 | 3.70 ± 0.068 | RNP | 0.77 ± 0.043 | 0.32 ± 0.006 | 3.49 ± 0.15 |
| GP | 24.9 ± 8.4 | 0.18 ± 0.004 | 2.64 ± 0.058 | GP | 0.59 ± 0.016 | 0.29 ± 0.008 | 1.25 ± 0.43 |
| GraphDF-RBF | 27.5 ± 2.1 | 0.17 ± 0.016 | 2.77 ± 0.049 | GraphDF- RBF | 0.61 ± 0.016 | 0.13 ± 0.002 | 0.96 ± 0.24 |
| GraphDF-Adj | 29.3 ± 2.4 | 0.21 ± 0.012 | 2.10 ± 0.037 | GraphDF- Adj | 0.52 ± 0.055 | 0.16 ± 0.005 | 1.68 ± 0.61 |
| DeepCovid | 26.4 ± 7.1 | 0.16 ± 0.009 | 2.83 ± 0.037 | EpiDeep | 0.93 ± 0.049 | 0.28 ± 0.007 | 3.16 ± 0.91 |
| CMU-TS | 19.4 ± 3.1 | 0.16 ± 0.017 | 2.63 ± 0.029 | EpiFNP | 0.31 ± 0.057 | 0.03 ± 0.002 | 0.37 ± 0.06 |
| CAMUL | 16.7 ± 8.8 | 0.09 ± 0.010 | 1.12 ± 0.035 | CAMUL | 0.19 ± 0.064 | 0.04 ± 0.004 | 0.35 ± 0.05 |
| CAMUL-C | 17.5 ± 3.5 | 0.12 ± 0.005 | 1.71 ± 0.021 | CAMUL-C | 0.26 ± 0.022 | 0.05 ± 0.001 | 0.39 ± 0.08 |
| CAMUL-S | 17.2 ± 4.6 | 0.14 ± 0.004 | 1.52 ± 0.035 | CAMUL-S | 0.25 ± 0.064 | 0.06 ± 0.006 | 0.41 ± 0.06 |
| CAMUL-D | 21.6 ± 8.4 | 0.21 ± 0.008 | 2.76 ± 0.038 | CAMUL-D | 0.62 ± 0.081 | 0.23 ± 0.002 | 1.27 ± 0.03 |
| | covid19 (3 week ahead) | | | google-symptoms (3 week ahead) | | | |
| | CRPS | CS | IS | CRPS | CS | IS | |
| SARIMA | 75 ± 2.6 | 0.44 ± 0.015 | 7.06 ± 0.033 | SARIMA | 1.94 ± 0.015 | 0.43 ± 0.014 | 6.49 ± 0.32 |
| DeepAR | 47.9 ± 5.2 | 0.24 ± 0.016 | 2.29 ± 0.027 | DeepAR | 1.43 ± 0.011 | 0.14 ± 0.008 | 3.38 ± 0.16 |
| DSSM | 55.9 ± 4.6 | 0.19 ± 0.012 | 3.08 ± 0.060 | DSSM | 1.53 ± 0.016 | 0.13 ± 0.005 | 3.76 ± 0.12 |
| RNP | 64.7 ± 7.1 | 0.34 ± 0.015 | 4.93 ± 0.051 | RNP | 1.05 ± 0.032 | 0.43 ± 0.003 | 3.72 ± 0.13 |
| GP | 33.8 ± 2.8 | 0.26 ± 0.014 | 3.83 ± 0.033 | GP | 1.43 ± 0.026 | 0.21 ± 0.009 | 2.21 ± 0.47 |
| GraphDF-RBF | 36.8 ± 1.6 | 0.19 ± 0.021 | 2.89 ± 0.036 | GraphDF- RBF | 1.47 ± 0.019 | 0.08 ± 0.005 | 2.53 ± 0.31 |
| GraphDF-Adj | 43.4 ± 4.7 | 0.24 ± 0.018 | 3.24 ± 0.010 | GraphDF- Adj | 1.58 ± 0.036 | 0.08 ± 0.004 | 3.15 ± 0.39 |
| DeepCovid | 46.2 ± 6.6 | 0.26 ± 0.009 | 3.71 ± 0.031 | EpiDeep | 1.13 ± 0.031 | 0.24 ± 0.013 | 6.35 ± 0.71 |
| CMU-TS | 32.3 ± 5.1 | 0.21 ± 0.016 | 3.80 ± 0.065 | EpiFNP | 0.72 ± 0.062 | 0.07 ± 0.003 | 0.83 ± 0.11 |
| CAMUL | 26.2 ± 6.3 | 0.14 ± 0.009 | 1.83 ± 0.014 | CAMUL | 0.46 ± 0.042 | 0.05 ± 0.007 | 0.68 ± 0.22 |
| CAMUL-C | 29.5 ± 4.6 | 0.17 ± 0.009 | 2.19 ± 0.022 | CAMUL-C | 0.57 ± 0.030 | 0.06 ± 0.003 | 0.76 ± 0.12 |
| CAMUL-S | 26.3 ± 1.4 | 0.19 ± 0.005 | 1.99 ± 0.042 | CAMUL-S | 0.54 ± 0.052 | 0.06 ± 0.011 | 0.71 ± 0.07 |
| CAMUL-D | 38.1 ± 5.1 | 0.26 ± 0.019 | 3.38 ± 0.035 | CAMUL-D | 1.15 ± 0.077 | 0.17 ± 0.007 | 2.86 ± 0.11 |
| | covid19 (4 week ahead) | | | google-symptoms (4 week ahead) | | | |
| | CRPS | CS | IS | CRPS | CS | IS | |
| SARIMA | 85.3 ± 3.9 | 0.43 ± 0.013 | 7.86 ± 0.038 | SARIMA | 2.31 ± 0.013 | 0.35 ± 0.006 | 7.72 ± 0.24 |
| DeepAR | 59.4 ± 5.0 | 0.19 ± 0.018 | 3.85 ± 0.021 | DeepAR | 1.42 ± 0.016 | 0.17 ± 0.004 | 5.63 ± 0.13 |
| DSSM | 68.2 ± 4.3 | 0.21 ± 0.014 | 3.16 ± 0.051 | DSSM | 1.57 ± 0.015 | 0.15 ± 0.002 | 4.91 ± 0.14 |
| RNP | 74.5 ± 6.4 | 0.33 ± 0.017 | 5.19 ± 0.044 | RNP | 1.27 ± 0.053 | 0.45 ± 0.008 | 4.13 ± 0.15 |
| GP | 58.7 ± 2.1 | 0.23 ± 0.016 | 4.11 ± 0.017 | GP | 1.37 ± 0.032 | 0.31 ± 0.008 | 3.80 ± 0.41 |
| GraphDF-RBF | 57.7 ± 2.3 | 0.21 ± 0.018 | 3.42 ± 0.036 | GraphDF- RBF | 1.53 ± 0.013 | 0.13 ± 0.006 | 2.79 ± 0.24 |
| GraphDF-Adj | 65.3 ± 3.0 | 0.20 ± 0.010 | 3.79 ± 0.023 | GraphDF- Adj | 1.64 ± 0.058 | 0.17 ± 0.003 | 2.87 ± 0.61 |
| DeepCovid | 56.3 ± 6.8 | 0.28 ± 0.014 | 4.57 ± 0.029 | EpiDeep | 1.27 ± 0.038 | 0.41 ± 0.011 | 8.41 ± 0.91 |
| CMU-TS | 47.0 ± 4.6 | 0.32 ± 0.016 | 3.62 ± 0.069 | EpiFNP | 0.75 ± 0.052 | 0.04 ± 0.004 | 0.93 ± 0.18 |
| CAMUL | 24.6 ± 4.4 | 0.19 ± 0.018 | 2.26 ± 0.028 | CAMUL | 0.48 ± 0.057 | 0.04 ± 0.002 | 0.71 ± 0.02 |
| CAMUL-C | 41.0 ± 3.3 | 0.25 ± 0.015 | 2.51 ± 0.019 | CAMUL-C | 0.64 ± 0.024 | 0.06 ± 0.006 | 0.75 ± 0.06 |
| CAMUL-S | 38.7 ± 3.6 | 0.21 ± 0.018 | 3.22 ± 0.043 | CAMUL-S | 0.56 ± 0.043 | 0.08 ± 0.008 | 0.83 ± 0.02 |
| CAMUL-D | 52.3 ± 8.3 | 0.34 ± 0.036 | 4.14 ± 0.025 | CAMUL-D | 1.44 ± 0.065 | 0.15 ± 0.006 | 2.99 ± 0.04 |

Table 6: Evaluation scores (over 20 runs) for CAMUL and baselines for all covid19 and google-symptoms for 1,3 and 4-week ahead targets. Similar to the results discussed in Section 5.1 Q1, our CAMUL significantly outperforms the state-of-art baselines and variants without dynamic view selection and stochastic view-specific uncertainty modelling.